Chinese Chemical Letters 36 (2025) 109797

Contents lists available at ScienceDirect

Chinese Chemical Letters

journal homepage: www.elsevier.com/locate/cclet

Single-atom Ti doping on S-vacancy two-dimensional CrS_2 as a catalyst for ammonia synthesis: A DFT study

Yiwen Xu[a], Chaozheng He[a,*], Chenxu Zhao[a,*], Ling Fu[b,*]

[a] Institute of Environment and Energy Catalysis, Shanxi Key Laboratory of Optoelectronic Functional Materials and Devices, School of Materials Science and Chemical Engineering, Xi'an Technological University, Xi'an 710021, China
[b] College of Resources and Environmental Engineering, Tianshui Normal University, Tianshui 741001, China

ARTICLE INFO

Article history:
Received 24 January 2024
Revised 15 March 2024
Accepted 19 March 2024
Available online 20 March 2024

Keywords:
CrS_2
NO electrocatalytic reduction
First principles calculation
Introducing vacancy doping

ABSTRACT

Electrocatalytic reduction of NO (NORR) is an effective method for NH_3 synthesis, due to low bonding energy of N–O bond. In this work, we have investigated many CrS_2 based catalysts, including pristine CrS_2, CrS_2 with one S vacancy (v-CrS_2), and Ti doped CrS_2 (Ti@CrS_2). The results have shown that the pristine CrS_2 exhibits inert character for NO activation. However, v-CrS_2 and Ti@CrS_2 can exhibit enhanced interaction with NO, due to increased charge transfer between NO and substrates (0.52–0.75 e) and enhanced adsorption energies of NO on the catalysts (-0.96∼-1.64 eV), compared to the situation of CrS_2 (0.065 e/-0.30 eV). From the free energy profiles of NO electro-reduction to NH_3, we can see that the v-CrS_2 and Ti@CrS_2 all exhibit ultralow limiting potentials of -0.03∼-0.47 V, following both *NOH and *NHO mechanisms. Therefore, introducing vacancy and doping are all promising modification strategies for NORR catalysts. The results have provided a new idea for the search of catalysts for efficient electrocatalytic reduction of NO.

NH_3, as one of the key chemicals for human production and life, plays a vital role in promoting human society through its application in agricultural production, chemical fuel, etc. Currently, the Haber-Bosch process is an industrial direct synthesis of ammonia from N_2 and H_2 under high temperature (300–500 °C) and high pressure (15,000–30,000 kPa) conditions. To meet the demanding conditions of high temperature and pressure in synthesis, large amounts of fossil fuels are consumed, so nearly 12% of the energy consumed in industrial ammonia synthesis is used annually, emitting over 300 million tons of carbon dioxide (CO_2), causing an energy resource crisis and global greenhouse effect. Therefore, in order to solve the problems of high energy consumption, high pollution and complex plant facilities in the Haber-Bosch process, there is an urgent need to develop a new process to replace the existing ammonia production method. Electrochemical nitrogen reduction (NRR) is a more environmentally friendly and economical method for synthesis. An increasing number of researchers have explored a variety of materials for catalytic nitrogen reduction reactions, providing theoretical guidance for the exploration of novel catalytic materials [1–10]. For example, Liu *et al.* [2] designed dual-dot metal-free atom catalysts anchored on g-CN. Based on DFT calculations, the limiting potential of the B and P co-doped g-CN system is as low as −0.18 V, which exhibits excellent NRR performance. Ma *et al.* [3] have discovered that the B dopant in InSe can effectively reduce N_2 to NH_3 under ambient conditions, because of the empty orbitals of B ions and the favorable carrier mobility of InSe. However, the strong bonding strength of the non-polar N≡N bond is extremely difficult to be destroyed at room temperature, leading to low reactivity in the process of ammonia synthesis. Compared to N_2, the NO molecule manifests a single unpaired electron in the π^* (π^*2py) orbital, leading to a relatively weaker binding strength of N–O bond. Therefore, it is easier to activate NO to synthesis ammonia, compared to the situation of N_2. Therefore, many pioneering studies have focused on the study of NO electroreduction (NORR), which is assumed to achieve higher reactivity compared to NRR.

Nitric oxide (NO) is a polluting gas produced by vehicle emissions and the burning of fossil fuels. Its large emission will not only pollute the environment but also threaten human health. At the same time, NO, as another nitrogen-containing gas molecule, acts as a free radical and can be used as a nitrogen source for catalytic reactions. In recent years, some scholars have tried to use NO as a nitrogen source to synthesize ammonia by electrocatalysis, which is called electrocatalytic nitric oxide electroreduc-

* Corresponding authors.
E-mail addresses: hecz2019@xatu.edu.cn (C. He), zhaochenxu@xatu.edu.cn (C. Zhao), ful263@nenu.edu.cn (L. Fu).

https://doi.org/10.1016/j.cclet.2024.109797
1001-8417/

tion reaction (NORR). NORR not only solves the problem that NO in the atmosphere is harmful to the environment and human health, but also provides a green synthesis method for NH_3 needed for industrial production [11–22]. For example, The experiments of Li *et al*. [17] revealed that the oxygen vacancy (VO) in MnO_2 nanowire arrays can efficiently activate NO and further reduce NO to NH_3, with a NH_3 yield of 27.51×10^{-10} mol s^{-1} cm^{-2} and a Faraday efficiency of 82.8%. Ji *et al.* [18] investigated the potential of boron-doped graphene (BG) as a metal-free catalyst for the catalytic reduction of ammonia by NO. Calculations, based on density functional theory (DFT), have showed that the introduction of B dopants into graphene can enhance its interactions with HNO* intermediates and effectively facilitates the subsequent reduction steps along the NH_2O*, NH_2OH*, and NH_2* intermediates, with a low limiting potential of −0.35 V. Chen *et al.* [21] designed the Co-N_4/graphene (The Co atom is anchored on porphyrin-like N-doped graphene) structure to study its catalytic performance. The results of DFT calculations show that the limiting potential of NORR on Co-N_4/graphene is −0.12 V, which is comparable (or even better) than that of metal Pt. Therefore, Co-N_4/graphene can be treated as a highly promising catalyst. These results have indicated that it is feasible to use NO as a nitrogen source in the process of ammonia synthesis, from both theoretical and experimental aspects.

In recent years, two-dimensional materials, such as graphene, hexagonal boron nitride, transition metal compounds, have been investigated extensively in the areas of energy and catalysis, due to their unique structures and excellent physical and chemical properties [23–38]. Among them, the unique layered structure of transition metal sulfides is often used as catalytic materials, benefiting from the unique configuration: The transition metal layer is sandwiched between two layers of sulfur atoms. For example, Ma *et al*. [4] have systematically investigated WS_2 nanosheet based single metal atoms as NRR catalysts. The results of DFT calculations show that WS_2 nanosheets with sulfur vacancies are good platforms for anchoring individual transition metal atoms. Among them, the Ni system (Ni-WS_2) has prominent NRR catalytic activity, and the NRR process on the Ni-WS_2 surface is more inclined to occur with the alternating hydrogenation-binding pathway and generates ammonia without energy input. Li *et al*. [39] designed two-dimensional transition metal disulfides, including MoS_2, WS_2, VS_2, NbS_2, TiS_2 and TaS_2, to study their NRR process. DFT-based calculations of energy barriers for each step show that VS_2 has 0.16 eV in the distal path, which endows it with favorable catalytic activity among the candidates investigated. In addition, the author has also demonstrated that charge transfer is crucial for the reactivity of NRR. Many researchers have also focused their studies on CrS_2, which is a novel metal disulfide. Chen *et al*. [40] studied disulfides based on transition metals in all groups, including IV, V and VI, and found that CrS_2 manifests the most diverse electronic and magnetic properties. Gabriela *et al*. [41] have also found that CrS_2 has the highest charge transfer efficiency, compared with MoS_2 and WS_2. Qin *et al*. [42] designed heteroatom-doped CrS_2 catalysts (X@CrS_2, X = B, C, N, O, Si, P, Cl, As, Se, and Br) to study their catalytic properties. Based on energy calculations, N@CrS_2 has the lowest overpotential (0.41 V) of NRR, which is even lower than that of Pt (0.45 V). Therefore, CrS_2 can be used as a promising catalyst.

As we know, some catalysts can be flexibly modulated *via* some strategies, which is beneficial for the improvement of reactivity. Among numerous methods, introducing vacancy defects and doping heterogeneous atoms are widely used [43–45]. For example, Tursun [19] have attempted to introduce S vacancies in MoS_2 to explore their NO catalytic reduction properties. The results of DFT calculations showed that the S vacancies can effectively activate NO with an extended N–O bond, which is beneficial for NO-catalyzed reduction. The high reactivity mainly originates from the strong interaction between NO and the catalyst, induced by the vacancy defects. Besides, the heteroatom doping can accelerate the NO-catalyzed process by modulating the electron-donating ability of the MoS_2 substrate. Among them, the onset potential of NH_3 production was −0.06 V on the Pt-doped MoS_2 catalyst with S vacancies. Therefore, the Pt-MoS_2@Vs catalysts have a great potential for catalyzing the reduction of ammonia from NO; Liu *et al*. [1] have systematically designed graphene based catalysts with various kinds of defects for NRR. The results have demonstrated that graphene containing one vacancy (GR1) and two vacancy (GR2) defects had higher reactivity and better adsorption stability than pristine graphene (GR). For elemental doped graphene, both N and S dopants can significantly improve the adsorption strength of NRR intermediates and further improve the NRR reactivity. Among numerous dopants, Ti can be treated as a promising candidate with cheap and easily obtained characters, which has been investigated extensively in pioneering works. For instance, Wang *et al*. [36] have performed DFT calculations on Ti doped two-dimensional (2D) boron nitride (BN). The Ti dopant can effectively reduce the energy barrier of ammonia synthesis from 1.20 eV (on pristine BN) to 0.96 eV, suggestion that Ti doped 2D materials have the potential to be new catalysts for electrocatalytic ammonia synthesis. Kalwar *et al*. [46] have also investigated hydrogen adsorption on Ti doped vacancy silicene (SV-SL) *via* first-principles density-functional theory (DFT). The results have demonstrated that the adsorption energies of H_2 ranges from −0.481 eV to −0.201 eV, with a hydrogen storage capacity of 6.3 wt%. This study suggests that the Ti doped 2D materials could also be a promising candidate for hydrogen storage applications. Liu *et al.* [47] designed a Ti doped BP monolayer with B vacancy (Ti@BP) for the application of NORR. Ti@BP is proved to manifest excellent NORR selectivity for NH_3, which is similar to that of the Pt-based catalysts. The above experimental calculations proved that both doping and manufacturing vacancies can significantly improve the catalytic performance of the catalyst. Above all, The Ti doped two-dimensional materials have achieved superior performance in the catalysis area due to moderate adsorption strength of intermediates. We therefore treat Ti as a promising dopant for two-dimensional catalysts.

Inspired by the pioneering studies, we have herein investigated catalysts for electrocatalytic reduction of NO, including pristine CrS_2, CrS_2 with one S vacancy (v-CrS_2), and Ti doped CrS_2 (Ti@CrS_2). The results have shown that the pristine CrS_2 exhibits inert character for NO activation. However, v-CrS_2 and Ti@CrS_2 can exhibit enhanced interaction with NO, due to increased charge transfer between NO and substrates (0.52–0.75 e) and enhanced adsorption of NO on the catalysts (−0.96∼−1.64 eV), compared to the situation of CrS_2 (0.065 e/−0.30 eV). The results, including adsorption energies and reaction pathways, have demonstrated that v-CrS_2 and Ti@CrS_2 can both be treated as promising catalysts for NORR, with ultralow limiting potentials of −0.03∼−0.47 V. Therefore, the strategies, including introducing vacancy and doping, are proved as effective methods to improve the reactivity of NORR. This study has provided a theoretical basis for the search of sulfide catalysts in the area of NO electroreduction.

In this work, the spin density functional theory is implemented by using the Vienna Ab initio Simulation Package (VASP). Projection enhanced wave (PAW) method is used to describe the interaction between ions and electrons. The generalized gradient approximation (GGA) of Perdew-Burke-Ernzerhof (PBE) functional is used to describe the exchange correlation. A $3 \times 3 \times 1$ CrS_2 supercell with S vacancy containing 9 Cr atoms and 18 S atoms was used for calculation. The cutoff energy was set as 450 eV. The vacuum layer was set as 15 Å to avoid periodic repetition effects. The Monkhorst Pack k-point grid of $5 \times 5 \times 1$ was chosen to sample the Brillouin zone for geometric optimization. The convergence criterion for the residual force and energy was set to 0.02 eV/Å and 10^{-5} eV, respectively.

The adsorption energy was calculated by Eq. 1:

$$E_{ads} = E_{slab/NO} - E_{slab} - E_{NO} \quad (1)$$

where the $E_{slab/NO}$, E_{slab} and E_{NO} are energies of catalyst with NO adsorbed on it, pure catalyst, and NO molecule in vacuum, respectively.

The reaction free energy (ΔG) of every reaction step was modified with the zero-point energy and entropy of DFT. The calculation formula follows Eq. 2:

$$\Delta G = \Delta E + \Delta ZPE - T\Delta S \quad (2)$$

ΔE is obtained from DFT calculations, ΔZPE is zero-point energy, T is 298.15 K and ΔS is entropy change.

Charge transfer indicates a change in the electronic structure of each adsorption system. The charge transfer is calculated as follows Eq. 3:

$$\Delta Q_c = Q_N + Q_O \quad (3)$$

ΔQ_c represents the charge transfer between NO and CrS_2, Q_N represents the charge of the N atom in NO after adsorption, and Q_O represents the charge of the O atom in NO after adsorption. If the calculated ΔQ_c is negative, NO gains electrons and CrS_2 loses electrons during adsorption. On the contrary, if ΔQ_c is positive, electrons are transferred from NO to CrS_2. In general, the amount of charge transfer indicates the adsorption capacity of the adsorbent for the adsorbate.

For v-CrS_2, the calculation of vacancy formation energy follows Eq. 4:

$$E_v = E_{defect} - E_{prefect} \quad (4)$$

where N is the total number of particles, $E_{prefect}$ is the total energy of the optimized cell, and E_{defect} is the total energy of the optimized cell containing vacancies.

For Ti@CrS_2, the calculation of formation energy follows Eq. 5:

$$\Delta E = E_{Ti@CrS_2} - E_{v@CrS_2} - E_{Ti} \quad (5)$$

$E_{Ti@CrS_2}$ represents the energy of Ti@CrS_2, $E_{v@CrS_2}$ represents the energy of CrS_2 containing S vacancies, and E_{Ti} represents the energy of Ti atom in vacuum.

For Ti the cohesive energy is calculated as follows Eq. 6:

$$E_c = E_{Ti-bulk}/n - E_{Ti-single} \quad (6)$$

In this work, we first analyze the geometric properties of CrS_2 based catalysts to demonstrate the potential application of CrS_2 based catalyst in NO electroreduction. We focus on the research of pristine CrS_2 (001), CrS_2 with S vacancy (denoted as v-CrS_2) and CrS_2 with Ti atom doped in the S vacancy (denoted as Ti@CrS_2), as shown in Fig. 1. The structure presents two atomic layers in a unit cell containing a total of 9 Cr atoms and 18 S atoms. The layer of Cr atoms in each of these cells is placed between two layers of S atoms, forming a pincer structure. In order to illustrate the stability of catalysts designed, we have also calculated the vacancy-formation energy (E_f) of v-CrS_2, and the binding energy (E_b) of Ti in Ti@CrS_2.

The formation energy of S vacancies in CrS_2 was calculated as −1.51 eV according to Eq. 4. The negative value of E_f indicates that S vacancy defects are easily formed in the crystal structure of CrS_2 in practical experiments; The binding energy of Ti atom in Ti@CrS_2 was calculated to be −7.17 eV according to Eq. 5. The ultra-negative value of E_b suggests that the S in the pristine CrS_2 can be easily substituted by the Ti atom in the real experimental work. As we know, the Ti single atoms are likely to aggregate into clusters due to a large surface energy. We therefore demonstrate the stability *via* comparison of binding energy and cohesive energies. The binding energy of Ti atoms in CrS_2 is −7.17 eV, which is significantly larger than the cohesive energy of Ti (−4.90 eV). Therefore, the binding strength of Ti atom is big enough to inhibit the aggregation of Ti atoms into clusters. In other words, the formation of titanium atoms is thermodynamically more favorable than that of clusters. These results have demonstrated that our designed catalysts are advisable for the application in the real electrochemical condition.

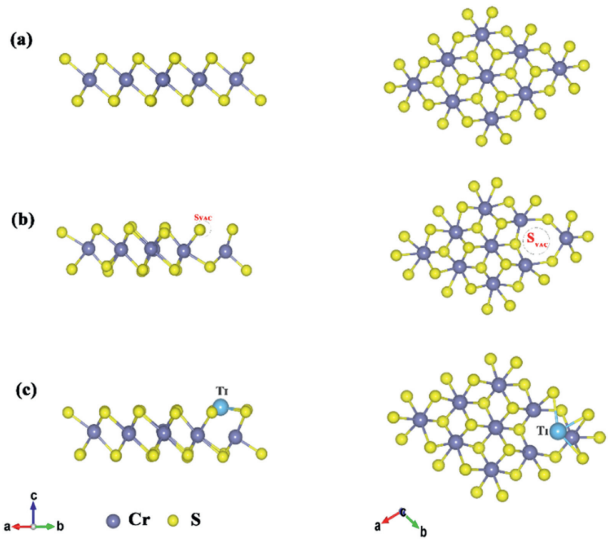

Fig. 1. Optimized geometrical structures of (a) CrS_2, (b) v-CrS_2, and (c) Ti@CrS_2. Cr, S and Ti atoms are represented by purple, yellow and pale bule, respectively.

Table 1
The properties of NO adsorbed on various systems, including CrS_2-S1, CrS_2-S2, v-CrS_2-S1, v-CrS_2-S2, Ti@CrS_2-S1, Ti@CrS_2-S2, and Ti@CrS_2-side. The E_{ads}[*NO] (Δd_{N-O} and ΔQ_c) indicates the adsorption energy of NO (the N–O bond length of adsorbed NO and the charge transfer between NO and the substrate).

Mode	E_{ads} (eV)	Δd_{N-O} (Å)	ΔQ_c (e)
CrS_2-S1	0.9215	−0.007	−0.042
CrS_2-S2	−0.304	−0.005	−0.065
V-CrS_2-S1	−1.643	0.026	0.752
V-CrS_2-S2	−0.981	0.097	0.515
Ti@CrS_2-S1	−1.178	0.070	0.536
Ti@CrS_2-S2	−0.694	0.054	0.368
Ti@CrS_2-side	−0.963	0.139	0.726

In addition, there are negligible structure deformation after introducing defects, including S vacancy and Ti dopant. This can further illustrate that CrS_2 is a stable substrate, which can effectively sustain the defect sites to avoid the deformation. To further determine the stability of v-CrS_2 and Ti@CrS_2, we performed calculations of phonon dispersion spectrum (Fig. S1 in Supporting information), the absence of imaginary frequencies in the phonon spectrum indicates that v-CrS_2 and Ti@CrS_2 manifest thermodynamic stability.

As we know, the prerequisite of NORR is the effective capture and activation of inert NO. We therefore focus on the discussion of NO adsorption on CrS_2. As shown in Fig. S2 (Supporting information), NO can be adsorbed on v-CrS_2 and Ti@CrS_2 spontaneously after full geometric optimization. Therefore, there exists no transition states in the process of NO adsorption. Based on the characters of the adsorbate and substrate, the NO can bind with CrS_2 vertically *via* both N (CrS_2-S1) and O (CrS_2-S2) atoms (Fig. 2a). According to Table 1 and Fig. 2a, NO prefers to be adsorbed on CrS_2 *via* CrS_2-S2 behavior with a low adsorption energy of −0.3 eV, indicating a physical adsorption character. This can also be reflected from the charge transfer, which is only −0.065 e between NO and CrS_2. Therefore, the interaction between NO and CrS_2 is extremely weak and NO cannot be effectively activated on CrS_2. We therefore

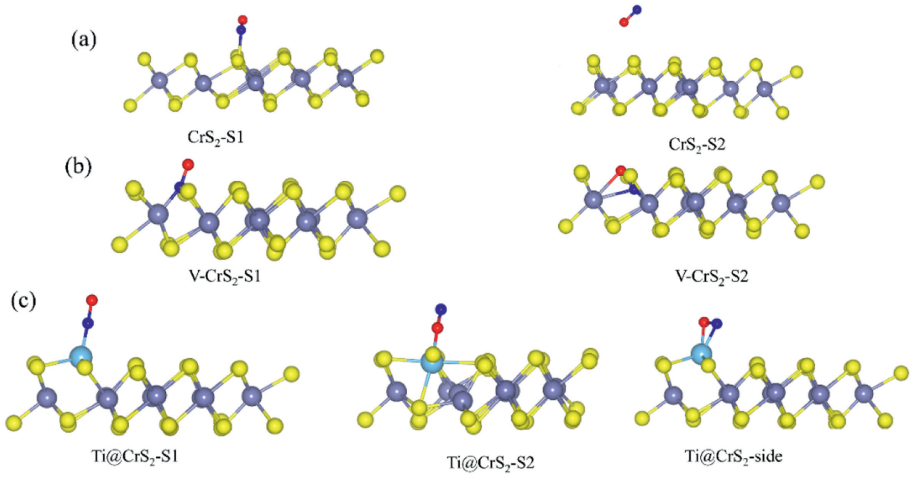

Fig. 2. The configurations of (a) CrS_2, (b) v-CrS_2, and (c) Ti@CrS_2, with NO adsorbed on them. The Cr, S, Ti, N and O atoms are denoted in the forms of purple, yellow, pale bule, bule, and red, respectively.

attempt to modify the CrS_2 with various defects, including vacancy and Ti dopant, to study further.

For v-CrS_2, we have also discussed various adsorption behaviors of NO on it, as pristine CrS_2. Based on the configuration of v-CrS_2, NO can be adsorbed on the S-vacancy vertically *via* N atom (v-CrS_2-S1) or parallelly *via* both N and O atoms (v-CrS_2-S2). As shown in Fig. 2b and Table 1, NO prefers to be adsorbed on v-CrS_2 *via* v-CrS_2-S1 behavior with an adsorption energy of −1.64 eV, which is significantly higher than that on pristine CrS_2 (−0.3 eV). Therefore, we can conclude that introducing S vacancy in CrS_2 is an effective strategy, which can dramatically enhance the interaction between NO and the catalyst. Similar conclusion can also be obtained from the aspect of charge transfer and change of N–O bond: The charge transfer between NO and v-CrS_2 ranges from 0.52 e to 0.75 e, which is remarkably larger than the situation of CrS_2 (−0.065 e). This may indicate that there exists a strong chemisorption between NO and CrS_2 surfaces. The adsorption energy of NO is −0.981 eV *via* v-CrS_2-S2 behavior on v-CrS_2, which also demonstrates a strong binding strength between NO and v-CrS_2.

Therefore, we can assume that the two adsorption behaviors of NO on v-CrS_2 are all likely to occur in the real electrochemical condition. In addition, the N–O bonds of adsorbed NO molecules are elongated by 0.026 and 0.097 Å respectively compared to the pristine state. This may further indicate that CrS_2 can effectively activate NO, which is beneficial for NO electroreduction. Above all, the v-CrS_2-S1 behavior is more beneficial for the capture NO due to a higher adsorption energy (−1.64 eV). In comparison, the v-CrS_2-S2 behavior can active NO more efficiently due to larger elongation of N–O bond (0.097 Å).

In order to demonstrate the phenomenon from the aspect of binding properties, we have calculated the crystal orbital Hamiltonian population (COHP) of N–O bond in adsorbed NO (Figs. 3a and b). To quantitatively analysis the occupation degree of NO's antibonding, we have also calculated the integrated COHP (ICOHP). The ICOHP values can reflect how much this bond contributes to the band-structure energy. ICOHP refers to the numerical integral from the lowest energy peak to 0 eV on the COHP. In general, the bonding (anti-bonding) state is defined as negative (positive) in COHP. Therefore, ICOHP can quantitatively indicate the occupation degree of anti-bonding states: A less negative ICOHP corresponds to a higher occupation degree of antibonding orbitals, leading to a more activated degree of NO. The ICOHP of adsorbed NO *via* v-CrS_2-S2 behavior is −7.96, which is more positive than the situation of v-CrS_2-S1 behavior (−9.22). We therefore assumed that the bidentate character of adsorbed NO *via* v-CrS_2-S2 is beneficial for the charge transfer between NO and v-CrS2 (0.75 e), which can further fill the antibonding orbitals of NO dramatically. This can effectively activate the adsorbed NO, leading to a significantly elongate N–O bond (0.097 Å). However, the occupation of NO antibonding states in v-CrS_2-S2 behavior will also lead to a destabilization of the system, leading to a decreased adsorption energy of NO (−0.981 eV), compared to the situation of v-CrS_2-S1 behavior (−1.64 eV). We have discussed the activation degree of NO from the aspect of N–O bond length, as mentioned above. However, the change of N–O bond length is not the only factor to determine the activation capacity. We therefore attempt to correlate the bond length with ICOHP to demonstrate the activation degree of NO. Among them, The ICOHP of NO adsorbed on v-CrS_2-S1 (v-CrS_2-S2, Ti@CrS_2-S1, and Ti@CrS_2-side) is −9.22 (−7.69, −9.07, and −7.02) with a N–O bond length of 0.026 Å (0.097 Å, 0.07 Å, and 0.139 Å). In general, a positive ICOHP corresponds to a more occupation degree of antibonding orbitals, which can lead to a more enlongation of N–O bond.

In order to further study the interaction between NO and v-CrS_2 (001) form the aspect of charge distribution, we have also calculated the charge differential density (CDD) (Figs. 4a and b). It can be clearly seen that both charge depletion and accumulation can be observed between NO and CrS_2, which is accordance with the well-known "accept-donate" mechanism as mentioned in pioneering works. In other words, the S vacancy not only transfers electrons to NO antibonding orbital, but also accepts lone pair electrons from NO molecule during NO activation. In general, the substrate is more capable of missing electrons, leading to the electron accumulation on NO. This is accordance with the bader charge analysis: The NO adsorbed on v-CrS_2 is negatively charged with −0.52∼−0.75 e. To further analyze the effect of S vacancies on the NO activation, we calculated the density of states (DOS) as shown in Fig. 5. Compared to pristine CrS_2, the upward and downward spin states of v-CrS_2 turn into asymmetric tendency near the Fermi energy level, indicating enhanced magnetism. This property can facilitate the transfer of electrons from v-CrS_2 to the empty orbitals of NO, filling the antibonding orbitals and favoring the activation of NO.

For Ti@CrS_2, we have considered three adsorption behaviors for NO: NO can be adsorbed on Ti@CrS_2 vertically with N (Ti@CrS_2-S1) or O (Ti@CrS_2-S2) atom. In addition, NO can also bond with Ti@CrS_2 parallelly with both N and O atoms (Ti@CrS_2-Side). As shown in Table 1 and Fig. 2c, the NO adsorbed *via* Ti@CrS_2-S1 and Ti@CrS_2-Side behaviors manifest higher adsorption energy

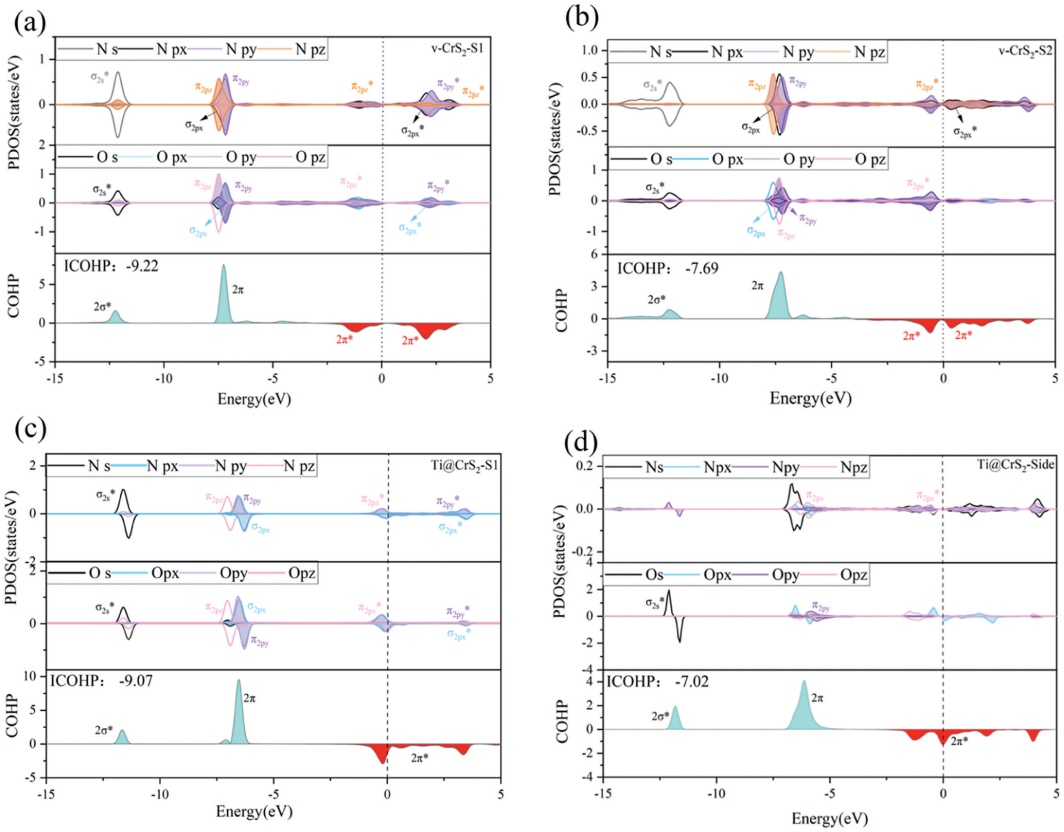

Fig. 3. Electron density of state projection (PDOS) and crystal orbital Hamiltonian population analysis (COHP) of adsorbed NO on systems, including (a) v-CrS_2-S1, (b) v-CrS_2-S2, (c) Ti@CrS_2-S1, and (d) Ti@CrS_2-Side, respectively.

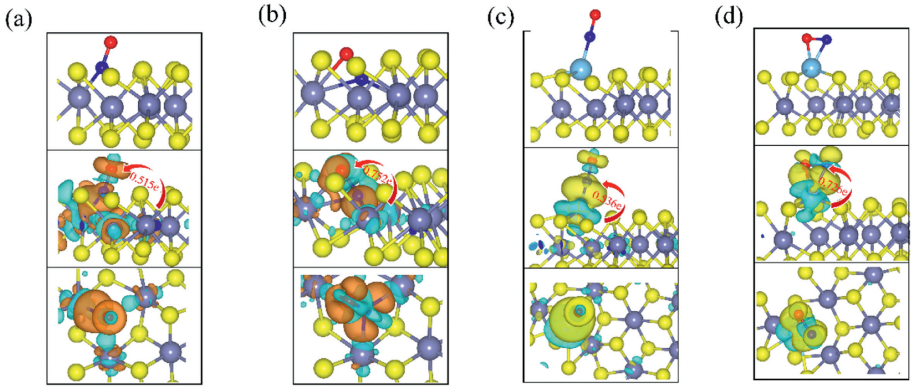

Fig. 4. The charge density difference between NO and substrates, including (a) v-CrS_2-S1, (b) v-CrS_2-S2, (c) Ti@CrS_2-S1, and (d) Ti@CrS_2-Side, respectively. The yellow (orange) and green areas denote the accumulation and depletion of charge, respectively. Cr, S, N and O atoms are denoted with the forms of purple, yellow, blue, and red, respectively.

of −0.963∼−1.178 eV, compared to the situation of Ti@CrS_2-S2 (−0.694 eV). From this phenomenon, we can deduce that the binding strength of N atom is stronger than the O atom for NO on Ti@CrS_2. Therefore, NO is preferred to be captured *via* Ti@CrS_2-S1 or Ti@CrS_2-Side behavior in the real electrochemical environment. The adsorption energy of NO on Ti@CrS_2 is significantly improved compared to that on CrS_2 (−0.3 eV), which is similar to the situation on v-CrS_2. Moreover, the charge transfer between NO and Ti@CrS_2 ranges from 0.536 e to 0.726 e for Ti@CrS2-S1 and Ti@CrS2-Side behaviors, which is significantly larger than that for CrS_2 (Figs. 4c and d). This may indicate a strong chemisorption between NO and Ti@CrS_2 surface, similar to the situation of v-CrS_2. Therefore, introducing Ti dopant is also a promising modification strategy for CrS_2 to activate NO. This can also be reflected from the N–O bond lengths for the adsorbed NO molecules, which are elongate by 0.07 Å (Ti@CrS_2-S1), 0.054 Å (Ti@CrS_2-S2), and 0.139 Å (Ti@CrS_2-Side), respectively, compared with the pristine state. This can further demonstrate that Ti@CrS_2 can effectively activate NO, which is favorable for the electroreduction of NO. Through comparison between Ti@CrS_2-S1 and Ti@CrS_2-Side behaviors of NO adsorbed on Ti@CrS_2, we can find that the Ti@CrS_2-S1 (Ti@CrS_2-Side) behavior is more favorable for the capture (activation) of NO, due to a larger adsorption energy (N–O elongation) of −1.178 eV (0.139 Å), compared to that of Ti@CrS_2-Side (Ti@CrS_2-S1). This phenomenon can also be analyzed from COHP calculation (Figs. 3c and d). The N–O bond of NO adsorbed *via* Ti@CrS_2-Side behavior possesses more positive ICOHP of −7.02, compared to the situation of Ti@CrS_2-S1 behavior. This can reflect that the antibonding orbitals of NO adsorbed *via* Ti@CrS_2-Side behavior have been dramatically filled, which can also be illustrated from the coordina-

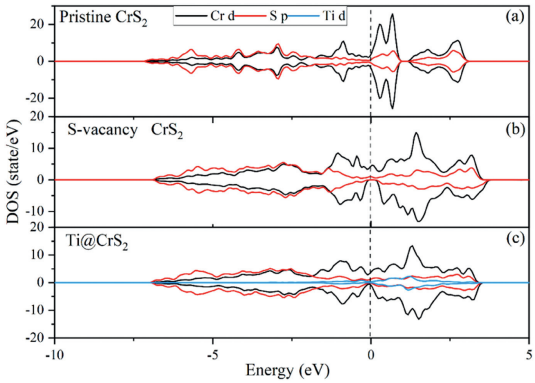

Fig. 5. The density of states of (a) pristine CrS_2, (b) v-CrS_2, and (c) Ti@CrS_2. The upper and lower panels indicate the upward and downward spin states, respectively. The Fermi energy level is set to zero.

tion aspect as the situation of v-CrS_2. As shown in Fig. 2c, the NO binds with Ti@CrS_2 bidentate (monodentate) with Ti@CrS_2 *via* Ti@CrS_2-Side (Ti@CrS_2-S1) behavior. The larger coordination number between Ti@CrS_2 and NO adsorbed *via* Ti@CrS_2-Side behavior can facilitate the charge transfer, as mentioned above. This will eventually lead to the significant occupation of NO's antibonding orbitals and weaken the N–O bond, corresponding to a larger N–O bond length. To further investigate the interaction between NO and Ti@CrS_2 from the aspect of charge distribution, we have also calculated the charge density difference (CDD), as shown in Figs. 4c and d. The interaction between NO and Ti@CrS_2 also follows the "accept-donate" mechanism, as analyzed above. The Ti doped in CrS_2 can transfer electrons to the antibonding orbitals of adsorbed NO, and simultaneously accept lone pair electrons from NO. This character eventually leads to efficient activation of NO during the interaction between the catalyst and NO. In general, the doped Ti atom is positively charged, consuming 1.41 e electrons to NO. In contrast, NO is negatively charged, accumulating 0.536 e electrons on it. Similar as the situation of v-CrS_2, the DOS of Ti@CrS_2 also exhibits an asymmetry tendency between upward and downward spin states, indicating an enhanced magnetism (Fig. 5). Therefore, the antibonding orbitals of NO adsorbed on Ti@CrS_2 can also be effectively filled, which can eventually facilitate the activation of NO.

As discussed above, the v-CrS_2 and Ti@CrS_2 are screened as promising catalysts for NO capture and activation, which has satisfied the prerequisite for ammonia synthesis. To analyze the reactivity quantitatively, we herein begin to discuss the hydrogenation process of NO to NH_3 (denoted as NORR). As discussed above, NO can be adsorbed on v-CrS_2 and Ti@CrS_2 *via* various behaviors due to similar adsorption strength. For v-CrS_2 (Ti@CrS_2), the v-CrS_2-S1 and v-CrS_2-S2 (Ti@CrS_2-S1 and Ti@CrS_2-side) behaviors of NO adsorption are all likely to occur in the real electrochemical condition, with high adsorption energies of −0.981∼−1.643 eV (−0.963∼−0.178 eV). In comparison, the coverage of N_2 with v-CrS_2-S2 (Ti@CrS_2-side) behavior is somewhat lower than that of v-CrS_2-S1 (Ti@CrS_2-S1) on v-CrS_2 (Ti@CrS_2), due to relative lower adsorption strength. Therefore, we focus our research on four systems, including v-CrS_2-S1, v-CrS_2-S2, Ti@CrS_2-S1, and Ti@CrS_2-side, to study the reaction pathway of NORR to NH_3.

As shown in Scheme 1, the adsorbed NO could be reduced to NH_3 *via* consumption of five hydrogen protons and electrons ($H^+ + e^-$) ($NO(g) + 5H^+ + 5e^- = NH_3(g) + H_2O(l)$) [18]. At each step of protonation, the proton-electron pair can selectively combine with the N- or O-terminal of NO, leading to various of mechanisms. The first protonation of NO is essential for the subsequent NORR process. *NO can be protonated into two different intermediates: HNO* and *NOH. Therefore, there are two possible reaction pathways for NORR: HNO* pathway and *NOH pathway. For v-CrS_2-S1 and Ti@CrS_2-S1 systems, the adsorbed *NO is unlikely to be protonated to *HNO, because the *NO is adsorbed on the substrate vertically with N atom binding on it. In comparison, the *NO is adsorbed on the substrate with parallel configurations in systems of v-CrS_2-S2 and Ti@CrS_2-side. Therefore, the *NOH and *HNO intermediates are all treated as possible intermediates for v-CrS_2-S2 and Ti@CrS_2-side systems. We first compare the free energy changes of the initial protonation steps: The reaction energy of $*NO \rightarrow *NOH$ is −0.66 eV/0.53 eV for v-CrS_2-S2/Ti@CrS_2-side system, which is much more negative (positive) than that of $*NO \rightarrow *HNO$ (0.16 eV/−0.82 eV). In summary, we eventually ignore *HNO (*NOH) and treat *NOH (*HNO) as the favorable intermediate in the subsequent research for the systems (system) of v-CrS_2-S1, v-CrS_2-S2, and Ti@CrS_2-S1 (Ti@CrS_2-side).

About *NOH pathway, the following protonation of *NOH can generate different intermediates, including *N and *HNOH, due to the selective combination with the N- or O-terminal. For *N intermediate, three proton-electron pairs are consumed successively until NH_3 is formed, which is defined as Path 1. In contrast, the further hydrogenation of *NHOH intermediate is still selective. As *NH is formed, it will experience two successive protonation steps to NH_3, which is defined as Path 2. When the intermediate is $*H_2NOH$, further protonation will lead to water generation to produce $*NH_2$ and NH_3, which is defined as Path 3. About *HNO pathway, *HNO can also be hydrogenated to various intermediates, including $*H_2NO$ and *HNOH, due to the selective combination with the N- or O-terminal. The further hydrogenation of $*H_2NO$ intermediate is still selective. As $*H_3NO$ is formed, it will be protonated first to produce NH_3 and *OH and further to H_2O, which is defined as Path 4. As the intermediate is H_2NOH*, it can be protonated to produce NH_3 and *OH as defined in Path 5. In addition, H_2NOH* can also be hydrogenated first to produce H_2O and $*NH_2$ further protonated to produce NH_3 as shown in Path 6. For the *HNOH intermediate, the formation of *NH followed by the consumption of two proton electron pairs to produce NH_3 is defined as Path 7. We next considered the further protonation of *NOH and *HNO by evaluating free energies of further reduction intermediates, and treat the reactions with lower free energies are more selective.

For v-CrS_2-S1 and v-CrS_2-S2 system, the minimum energy pathway can be demonstrated as follows: $*NO \rightarrow *NOH \rightarrow *N \rightarrow *NH \rightarrow *NH_2 \rightarrow *NH_3$ (Figs. S3a and b in Supporting information). It is noteworthy that the intermediates, including *HNOH, $*H_2NOH$ are all energetically unfavorable. For v-CrS_2-S1 (v-CrS_2-S2) system, the rate controlling step (RCS) of NORR is $*NO+H^+ + e^- \rightarrow *NOH$ ($*NH_2 + H^+ + e^- \rightarrow *NH_3$) with a reaction energy of 0.13 eV (0.37 eV), as shown in Figs. 6a and b. This reaction energy can be easily overcome at an ultralow limiting potential of −0.13 V (−0.37 V).

For Ti@CrS_2-S1 system, the minimum energy pathway is demonstrated as follows: $*NO \rightarrow *NOH \rightarrow *HNOH \rightarrow *NH \rightarrow *NH_2 \rightarrow *NH_3$ (Figs. S3c in Supporting information). The intermediates of *N and $*H_2NOH$ are energetically unfavorable. The rate controlling step (RCS) of NORR $*NH_3 \rightarrow NH_3(g)$ with a reaction energy of 0.47 eV, as shown in Fig. 6c. This reaction energy can be easily overcome at a limiting potential of −0.47 V.

For Ti@CrS_2-Side system, the favorable pathway can be described as: $*NO \rightarrow *HNO \rightarrow *H_2NO \rightarrow *H_2NOH \rightarrow *NH_3 + *OH \rightarrow *H_2O$ (Fig. S3d in Supporting information). The intermediates, including *HNOH, $*H_2NO$, and *NH, are unfavorable from energetic aspect. As shown in Fig. 6d, the rate controlling step (RCS) of NORR is $*OH + H^+ + e^- \rightarrow *H_2O$ with a reaction energy of 0.03 eV, which can be easily overcome at an ultralow limiting potential of −0.03 V.

Above all, the free energy profiles have demonstrated that both v-CrS_2 and Ti@CrS_2 can effectively activate NO to produce NH_3

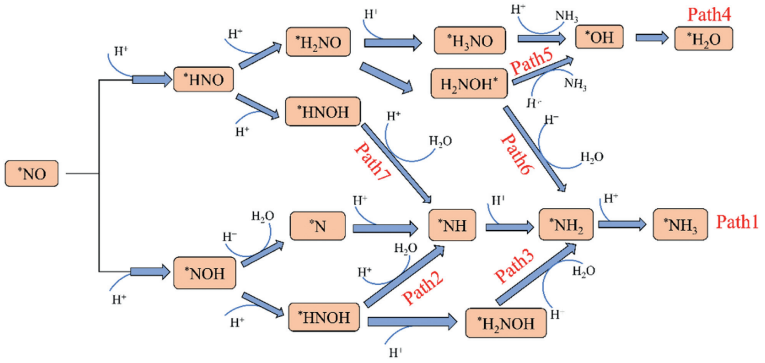

Scheme 1. The reaction pathway of NO reduction.

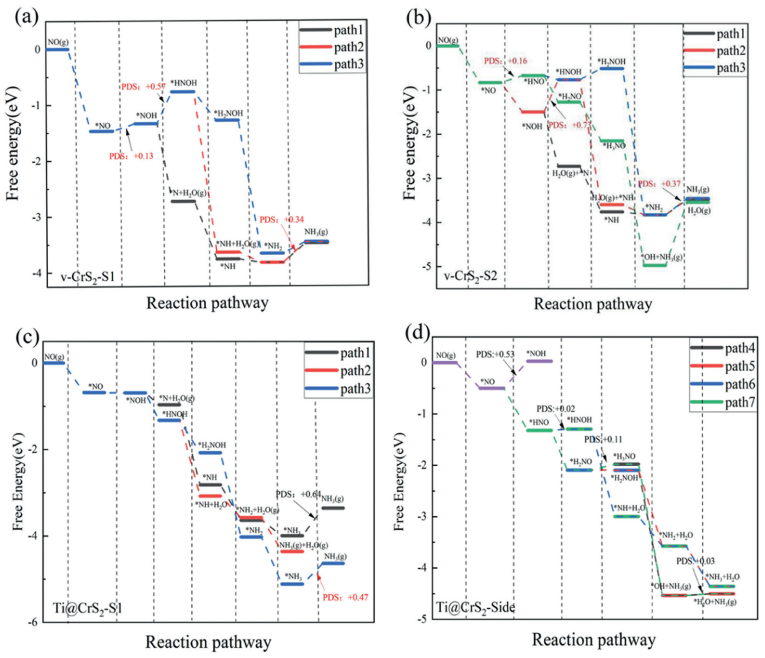

Fig. 6. The reaction pathway of NO reduction on systems of (a) v-CrS_2-S1, (b) v-CrS_2-S1, (c) Ti@CrS_2-S1, and (d) Ti@CrS_2-Side.

at the limiting potentials of −0.03 ∼ −0.47 V, with different reaction mechanisms. The configurations of intermediates of rate-controlling steps are demonstrated in Fig. S4 (Supporting information).

As we know, *H may also adsorbe on the catalysts by consuming the proton-electron pair and undergo a potential unwanted hydrogen evolution reaction (HER) side reaction. We thus calculated HER as an important side reaction in the process of NORR on v-CrS_2 and Ti@CrS_2. The *H adsorption free energy (ΔG_H) is a commonly used reactivity measure for HER, which is 1.10 eV and −0.63 eV on v-CrS_2 and Ti@CrS_2 respectively. Through the comparison of the limiting potentials between the NORR (−0.03 ∼ −0.47 V) and HER (−0.63 ∼ −1.10 V) (Fig. S5 in Supporting information), we find that our designed catalysts all prefer NORR to the HER, indicating a perfect selectivity.

In summary, we have herein investigated the electrocatalytic reduction of NO on catalysts, including CrS_2, v-CrS_2, and Ti@CrS_2 surfaces. The results have shown that the pristine CrS_2 exhibits inert character for NO activation. However, v-CrS_2 and Ti@CrS_2 can exhibit enhanced interaction with NO, due to increased charge transfer between NO and substrates (0.52∼0.75 e) and enhanced adsorption of NO on the catalysts (−0.96∼−1.64 eV), compared to the situation of CrS_2 (0.065 e/−0.30 eV). Based on the adsorption energies and ICOHP values, we eventually screen the systems, including v-CrS_2-S1 (E_{ads}[NO] = −1.64; ICOHP = −9.22), v-CrS_2-S2 (E_{ads}[NO] = −0.98 eV; ICOHP = −7.69), Ti@CrS_2-S1 (E_{ads}[NO] = −1.18 eV; ICOHP = −9.07), and Ti@CrS_2-side (E_{ads}[NO] = −0.96 eV; ICOHP = −7.02), as the favorable candidates, which are all likely to occur in the real electrochemical condition. From the free energy profiles of NO electro-reduction to NH_3, we can see that the systems of v-CrS_2-S1, v-CrS_2-S2, and Ti@CrS_2-S1 (Ti@CrS_2-Side) follow the *NOH (*NHO) mechanism, with ultralow limiting potentials of −0.03∼−0.47 V. We therefore assume that the methods, including introducing vacancy and doping, can be treated as promising modification strategies of CrS_2 for NO activation to synthesis NH_3. This study has provided a theoretical basis for the search of sulfide catalysts in the area of NO electroreduction.

Declaration of competing interest

All authors declared that there are no competing interests.

CRediT authorship contribution statement

Yiwen Xu: Data curation. **Chaozheng He:** Supervision. **Chenxu Zhao:** Investigation. **Ling Fu:** Investigation.

Acknowledgments

This study was funded by the Natural Science Foundation of China (No. 21603109), the Henan Joint Fund of the National Natural Science Foundation of China (No. U1404216), the Scientific Research Program Funded by Shaanxi Provincial Education Department (No. 20JK0676). This work was also supported by Natural Science Basic Research Program of Shanxi (Nos. 2022JQ-108, 2022JQ-096).

Supplementary materials

Supplementary material associated with this article can be found, in the online version, at doi:10.1016/j.cclet.2024.109797.

References

[1] A. Liu, Y. Yang, D. Kong, et al., Appl. Surf. Sci. 536 (2021) 147851.
[2] X. Liu, Y. Zhang, T. Liu, et al., Appl. Surf. Sci. 605 (2022) 154831.
[3] B. Ma, Y. Peng, D. Ma, Z. Deng, Z. Lu, Appl. Surf. Sci. 495 (2019) 143463.
[4] X.G. Ma, J.S. Hu, M.K. Zheng, et al., Appl. Surf. Sci. 489 (2019) 684–692.
[5] B. Castellano-Varona, M. Harb, J. Arana, L. Cavallo, L.M. Azofra, Chem. Commun. 56 (2020) 13343–13346.
[6] S.Y. Lv, C.X. Huang, G. Li, L.M. Yang, ACS Appl. Mater. Interfaces 13 (2021) 29641–29653.
[7] L. Xu, L.M. Yang, E. Ganz, ACS Appl. Mater. Interfaces 13 (2021) 14091–14101.
[8] Z. Wei, J. He, Y. Yang, et al., J. Energy Chem. 53 (2021) 303–308.
[9] Z. Xue, X. Zhang, J. Qin, R. Liu, J. Energy Chem. 57 (2021) 443–450.
[10] Y. Abghoui, A.L. Garden, J.G. Howalt, T. Vegge, E. Skúlason, ACS Catal. 6 (2016) 635–646.
[11] P. Liu, J. Liang, J. Wang, et al., Chem. Commun. 57 (2021) 13562–13565.
[12] Z. Lang, J. Miao, H. Tan, et al., Inorg. Chem. Front. 7 (2020) 4507–4516.
[13] T. Mou, J. Liang, Z. Ma, et al., J. Mater. Chem. A 9 (2021) 24268–24275.
[14] Y. Bai, M. Mavrikakis, J. Phys. Chem. B 122 (2018) 432–443.
[15] L. Ling, Z. Zhao, X. Feng, et al., J. Phys. Chem. C 121 (2017) 16399–16414.
[16] X.Y. Xie, Q. Wang, W.H. Fang, G. Cui, J. Phys. Chem. C 121 (2017) 16373–16380.
[17] Z. Li, Z. Ma, J. Liang, et al, Mater. Today Phys. 22 (2021) 100586.
[18] S. Ji, J. Zhao, New J. Chem. 48 (2018) 16346–16353.
[19] M. Tursun, C. Wu, Phys. Chem. Chem. Phys. 23 (2021) 19872–19883.
[20] Y. Xiao, C. Shen, Small 17 (2021) 2100776.
[21] Z. Wang, J. Zhao, J. Wang, C.R. Cabrera, Z. Chen, J. Mater. Chem. A 6 (2018) 7547–7556.
[22] C. He, R. Sun, L. Fu, et al., Chin. Chem. Lett. 33 (2021) 527–532.
[23] K. Chu, Y.P. Liu, Y.B. Li, Y.L. Guo, Y. Tian, ACS Appl. Mater. Interfaces 12 (2020) 7081–7090.
[24] X. Zhang, T. Wu, H. Wang, et al., ACS Catal. 9 (2019) 4609–4615.
[25] Y. Li, C. Cheng, S. Han, et al., ACS Energy Lett. 7 (2022) 1187–1194.
[26] H. Wan, A. Bagger, J. Rossmeisl, Angew. Chem. Int. Ed. 60 (2021) 21966–21972.
[27] S. Lu, F. Luo, Z. Yu, Catalysts 12 (2022) 228.
[28] C. Martín, K. Kostarelos, M. Prato, A. Bianco, Chem. Commun. 55 (2019) 5540–5546.
[29] X. Sun, L. Shi, H. Huang, X. Song, T. Ma, Chem. Commun. 56 (2020) 11000–11013.
[30] H. Bergeron, D. Lebedev, M.C. Hersam, Chem. Rev. 121 (2021) 2713–2775.
[31] Y. Wang, Z. Zhang, Y. Mao, X. Wang, Energy Environ. Sci. 13 (2020) 3993–4016.
[32] Y. Zhang, P. Liu, X. Zhu, Z. Liu, Int. J. Hydrog. Energy 46 (2021) 32936–32948.
[33] X. Hu, S. Guo, S. Zhang, et al., J. Mater. Chem. A 7 (2019) 25887–25893.
[34] T. Sun, G. Zhang, D. Xu, et al., Mater. Today Energy 12 (2019) 215–238.
[35] B. Luo, G. Liu, L. Wang, Nanoscale 8 (2016) 6904–6920.
[36] Y. Wang, Y. Du, Y. Meng, et al., Appl. Surf. Sci. 563 (2021) 150277.
[37] D. Zhou, C. Li, F. Yin, et al., Chin. Chem. Lett. 31 (2020) 2325–2329.
[38] C. He, J. Wang, L. Fu, W. Wei, Chin. Chem. Lett. 35 (2023) 109037.
[39] F. Li, L. Chen, H. Liu, et al., J. Phys. Chem. C 123 (2019) 22221–22227.
[40] K. Chen, J. Deng, Y. Yan, et al., npj Comput. Mater. 7 (2021) 79.
[41] G.B.M. Stan, K. Dhaka, M.C. Toroker, Israel J. Chem. 60 (2019) 888–896.
[42] Z. Qin, Z. Wang, X. Li, et al., Nanomaterials 12 (2022) 3012.
[43] Q. Wang, Q. Feng, Y. Lei, et al., Nat. Commun. 13 (2022) 3689.
[44] Q. Wang, S. Tang, Z. Wang, et al., Adv. Funct. Mater. 33 (2023) 2307390.
[45] H. Zheng, S. Wang, S. Liu, et al., Adv. Funct. Mater. 33 (2023) 2300815.
[46] B.A. Kalwar, W. Zong, I. Ahmed, M.H. Saeed, J. Chin. Chem. Soc. 68 (2021) 2243–2253.
[47] S. Liu, G. Xing, J. Liu, Appl. Surf. Sci. 611 (2022) 155764.